Supplementary Material

Discovery of a polyesterase from *Deinococcus maricopensis* and comparison to the benchmark LCC[ICCG] suggests high potential for semi-crystalline postconsumer PET degradation

Konstantinos Makryniotis[1], Efstratios Nikolaivits[1*], Christina Gkountela[2], Stamatina Vouyiouka[2], and Evangelos Topakas[1*]

[1]*Industrial Biotechnology & Biocatalysis Group, Biotechnology Laboratory, School of Chemical Engineering, National Technical University of Athens, Athens, Greece*

[2]*Laboratory of Polymer Technology, School of Chemical Engineering, National Technical University of Athens, Athens, Greece*

*Correspondence to: E. Topakas; vtopakas@chemeng.ntua.gr and E. Nikolaivits; snikolai@chemeng.ntua.gr

Supplementary Material

S1. Supplementary discussion

S1.1 Biochemical characterization of *Dm*PETase and LCC[ICCG]

Determined MWs of *Dm*PETase and LCC[ICCG], at 31 kDa and 29 kDa respectively (Figure S5), come to an agreement with the theoretical ones calculated through ExPASy ProtParam tool [1], at 30827 Da for *Dm*PETase and 28834 Da for LCC[ICCG].

*Dm*PETase acts optimally at 50 °C, with the enzyme retaining over 60 % of its maximum activity within a temperature range of 10 °C around this optimal temperature (Figure 2A). In comparison, LCC[ICCG] achieves maximum activity at 60 °C, maintaining 50 % of this activity within a temperature range of 20 °C around this value (Figure 2A). *Dm*PETase was stable for 3 days at temperatures ranging from 20 °C up to 50 °C, retaining over 70 % of its activity (Figure 2C). At 60 °C, the enzyme remained active after 1 h, but was completely deactivated after 8 h. At higher temperatures of 70 °C and 80 °C, *Dm*PETase retained less than 20 % of its activity after 1 h. The thermal stability of LCC[ICCG] was confirmed, with 70 % of its activity remaining after 3 days of incubation at 60 °C, and roughly 55 % and 65 % remaining activity at 70 °C and 80 °C, respectively (Figure 2D).

Regarding pH, *Dm*PETase showed maximum activity at pH 6.0 (C-P), with approximately 70 % activity retained at pH 7.0 (Figure 2B). The enzyme lost significant activity at slightly acidic (pH 5.0) or alkaline (pH 8.0-9.0) pH values, in the ballpark of 60 % and above. Conversely, LCC[ICCG] exhibited maximum activity at pH 8.5 with roughly 80 % activity at pH 8.0 and 9.0 (Figure 3). The stability of *Dm*PETase increased from acidic to alkaline pH, with maximum stability observed for T-H buffer system pH 9.0 (Figure S6). On the contrary, G-N buffer system at alkaline pH values compromised the stability of the enzyme. LCC[ICCG] stability was, favored at T-H pH 9.0 buffer, while P-P buffer systems of slight acidic to neutral pH negatively affected LCC[ICCG] stability (Figure S6). In fact, for the majority of the tested buffer systems the enzyme was more stable compared to the standard storage buffer.

The determination of kinetic constants for both *Dm*PETase and LCC[ICCG] (Table 1) on *p*NPA, *p*NPB, *p*NPO and *p*NPD indicated a typical Michaelis-Menten profile. The affinity of *Dm*PETase, was highest with *p*NPB, and 4- and 6-fold lower with *p*NPA-*p*NPD and *p*NPO, respectively. The highest k_{cat} for *Dm*PETase was observed for *p*NPB, which was almost the same as for *p*NPA, but significantly decreased with increasing substrates' acyl chain length, reaching a 15-fold drop for *p*NPD. According to these results, *Dm*PETase showed the highest

catalytic efficiency (k_{cat}/K_M) towards pNPB followed by pNPA, pNPO and pNPD. Concerning LCC^{ICCG}, the enzyme displayed major affinity for pNPB, followed by pNPD, pNPA and pNPO. Enzyme's k_{cat} was the highest for pNPA, decreasing with increasing chain length, resulting in a 20-fold drop for pNPD. The catalytic efficiency of LCC^{ICCG} peaked towards pNPB followed by pNPA, pNPO and pNPD, with a significant difference, around 60-fold lower.

Both DmPETase and LCC^{ICCG} have similar biochemical properties. They exhibit a thermophilic profile, being preferably active and stable at higher temperatures, with LCC^{ICCG} exhibiting superior thermotolerance. Although their optimum pH values might differ, they both work efficiently at neutral pH (70 % of the optimum), whereas their stability is favored at alkaline pH of 9.0 in the presence of Tris-base ions. The optimum conditions of DmPETase could be associated with the thermo-philic/tolerant nature of the microorganism of origin, being isolated from desert soil [2], while the stability of the enzyme at alkaline pH is justified, as studies of different soil samples from Sonoran Desert showed an average pH value near 9.0 [3]. The optimal activity conditions of LCC^{ICCG} are partially consistent with the findings of Sulaiman et al. and Su et al., who studied the wild-type LCC and its ICCG variant, respectively, demonstrating optimum activity at 50 °C and pH 8.0-8.5. According to recent studies [4,5], LCC^{ICCG} stability was only minimally affected (minimum relative activity 70 %) at 50 °C -70 °C for up to 8 h incubation, which accords with our results. Both DmPETase and LCC^{ICCG} show similar catalytic efficiency on pNPB ($K_{M,Dm\text{PETase}}$=158.8 mM^{-1}s^{-1}, $K_{M, LCC}^{ICCG}$ = 180.1 mM^{-1}s^{-1}), while DmPETase is 1.4-fold more efficient on pNPA and, LCC^{ICCG} slightly more active on pNPO, presenting 1.6-fold higher efficiency, but similar efficiency on pNPD (Table 1).

S1.2 Properties of tested polymeric materials

Two highly crystalline (cPET and bPET) and an amorphous PET (aPET) were the virgin grades, selected as the extreme cases of crystallinity. cPET and bPET presented the highest x_{c1} values of 40 % and 36 %, respectively (Table S1). These values were high enough for our analysis, given that the post-consumer PET packaging products typically present crystallinity higher than 20 % [9,10], about 35 % [11]. During the first heating, typical glass transition temperatures (T_{g1}) of 81-82°C were monitored for cPET and bPET [12], and a double melting behavior with melting points at 237 and 249-250°C (Figure S7, A). The double (or multiple) melting behavior of PET is a typical phenomenon strongly dependent on the material's thermal history [13]. It is mainly attributed to different distributions of lamella thickness and/or melting

Supplementary Material

and recrystallization (reorganization) of crystallites formed at low temperatures during the heating scan [13,14]. During cooling from the melt, cPET and bPET presented similar T_c and x_c (26 and 23 %, respectively). Single melting points were monitored (T_{m2} 248-249°C, which is typical for PET) [15] during the second heating, as cPET and bPET had enough time to crystallize during cooling, and probably no significant recrystallization occurred.

Regarding aPET powder, a sharp T_{g1} was monitored at 77 °C during the first heating indicating the amorphous character, which was confirmed by the calculated x_{c1} (i.e., 6 %), the lowest of all the examined materials. Cold crystallization occurred at 145 °C, followed by melting (T_{m1} 256 °C), a typical behavior of amorphous polymers. Crystallization from the melt occurred during cooling at 197 °C (Figure S7, B), followed by melting during the second heating. The T_{g2} was weak and thus unable to be defined during the second heating (Figure S7, C), while the calculated x_{c2} was about 28 %.

All the post-consumer PET bottle pieces and powders presented mass fraction crystallinity values between the limiting cases aPET (x_{c1} 6 %) and cPET, bPET (x_{c1} 40 %, 36 %). The transparent and green bottles' bottom (tbtPET and gbtPET), body (tbdPET and gbdPET) and shoulder (tsPET and gsPET) reached higher x_{c1} values (27-31 %) compared to the necks (tnPET and gnPET) that presented x_{c1} of 10-11 %. This difference is due to the manufacturing process of the bottles (i.e., blow molding), which results in stress-induced crystallization and macromolecular orientation in a parallel fashion regarding of the stretched parts of the bottles (bottom, body, shoulder) [16,17]. The bottles' powders (tPET and gPET) presented x_{c1} of about 21 %, between the neck and the stretched parts' mass fraction crystallinity, as expected. All the post-consumer PET grades presented decreased T_{g1} (73-76 °C) compared to the virgin semi-crystalline grades (cPET and bPET), probably indicating water-induced plasticization [18], considering the continuous contact of the products with water during usage. The monitored T_{g2} were higher (80-81 °C), as residual moisture was probably removed during the first heating. All the post-consumer grades crystallized during cooling at 179-188 °C ($x_c \sim$ 22-27 %) and presented similarly single melting points of 250-255°C during the first and the second heating (Figures S8 and S9).

Overall, across all tested PET samples, a range of crystallinity degrees, spanning from low (6 %) to high (40 %), was observed. All other thermal properties presented significant similarities, besides slightly decreased, T_{g1} of post-consumer PET grades compared to virgin grades, within rational bounds.

Supplementary Material

Except from PET, investigated target polyester (PBS, PCL, PHB, PLA) and polyurethane (PU) based polymers' properties (Table S2) were retrieved by Nikolaivits et al. [19], whose study was conducted using the exact same material grades.

S2. Supplementary Figures and Tables
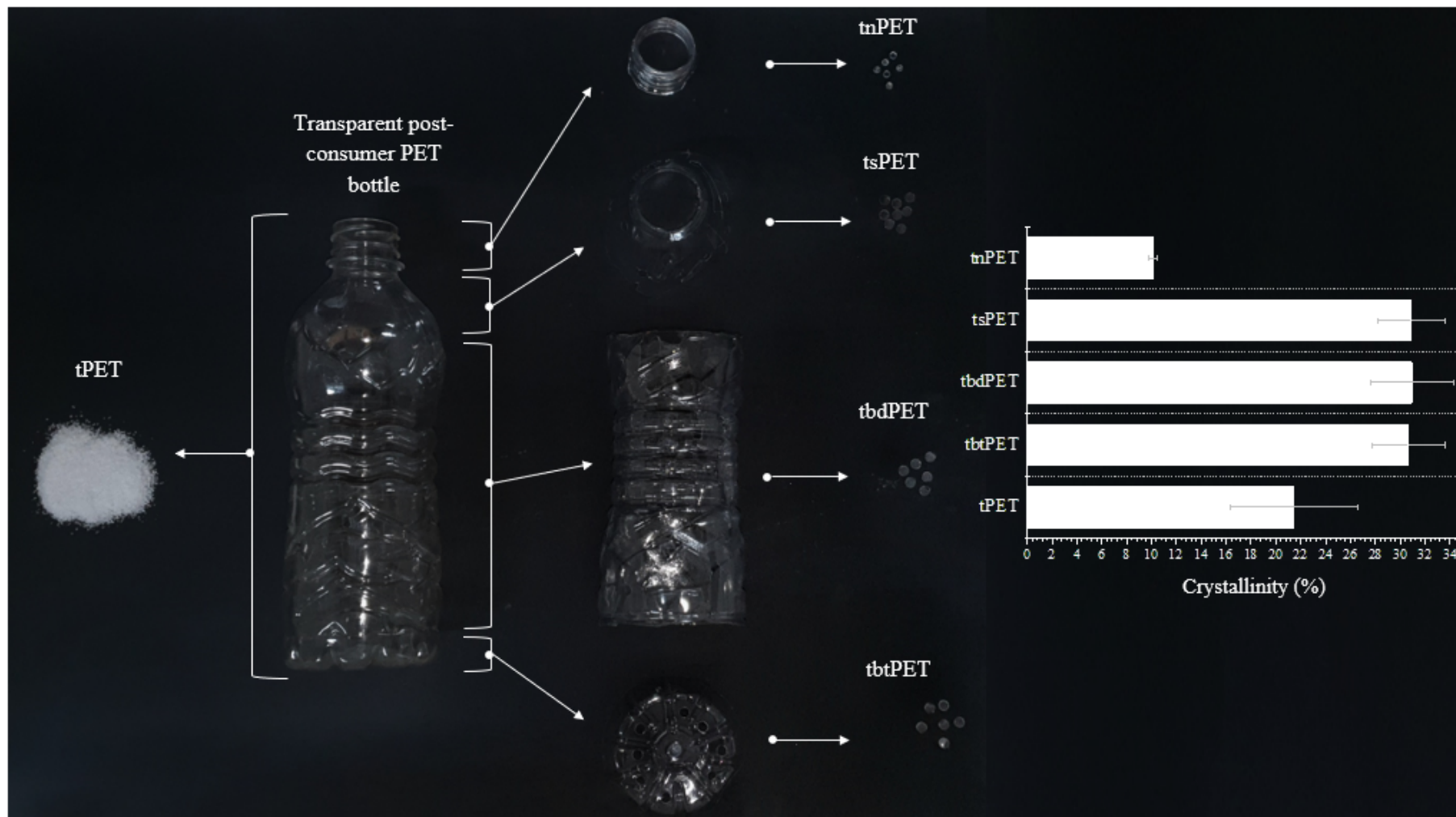
1 **Figure S1** Different investigated forms of post-consumer transparent PET bottle and their crystallinity grade: Whole transparent PET bottle

2 grinded into powder (tPET of x_c 21%), hole-punched chips from bottle's neck (tnPET of x_c 10%), shoulder (tsPET of x_c31%), body (tbdPET of

3 x_c35%) and bottom (tbtPET of x_c 33%).
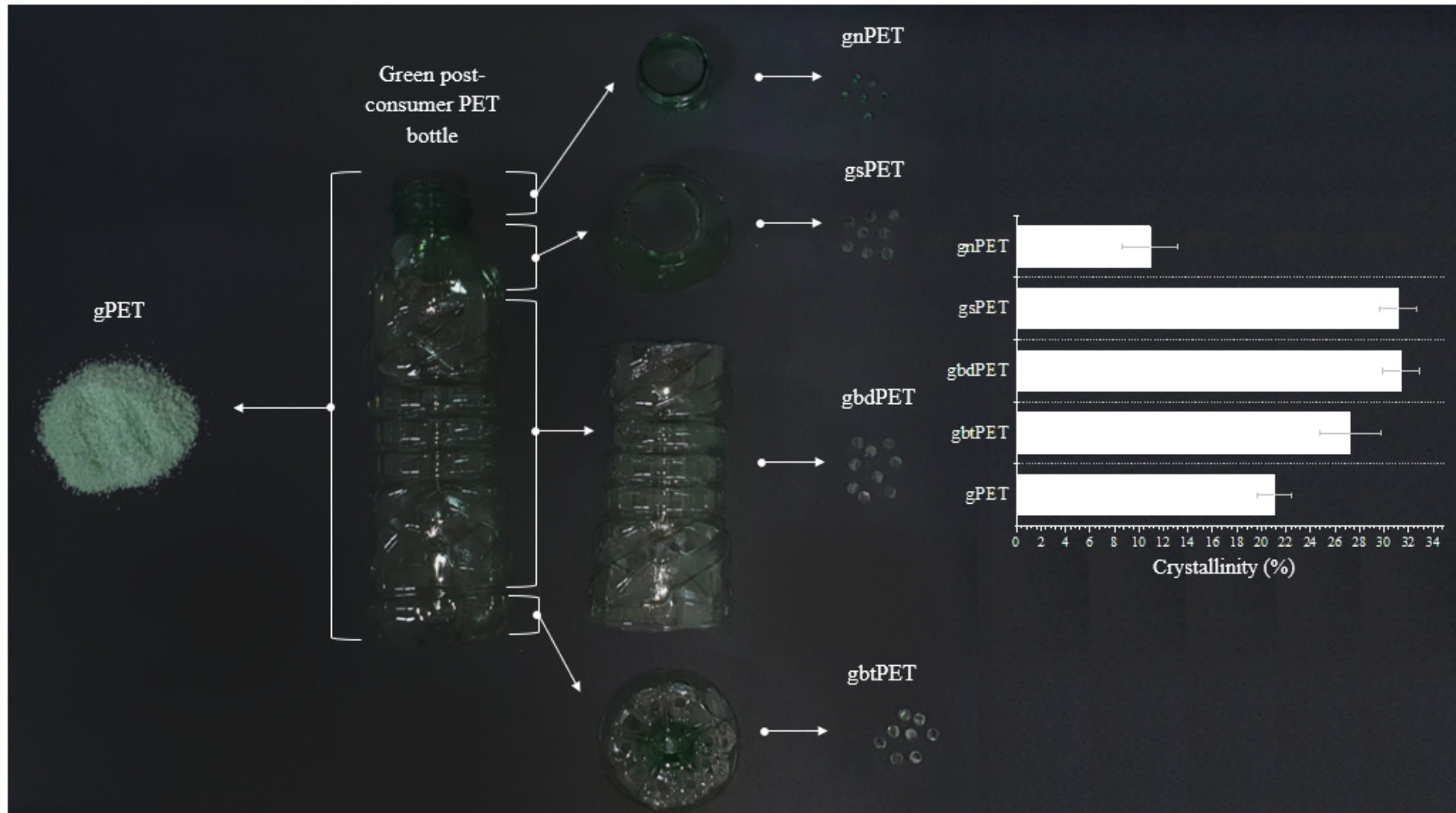
Figure S2 Different investigated forms of post-consumer green PET bottle and their crystallinity grade: Whole green PET bottle grinded into powder (gPET of x_c 21%), hole-punched chips from bottle's neck (gnPET of x_c 13%), shoulder (gsPET of x_c 31%), body (gbdPET of x_c 30%) and bottom (gbtPET of x_c 29%).
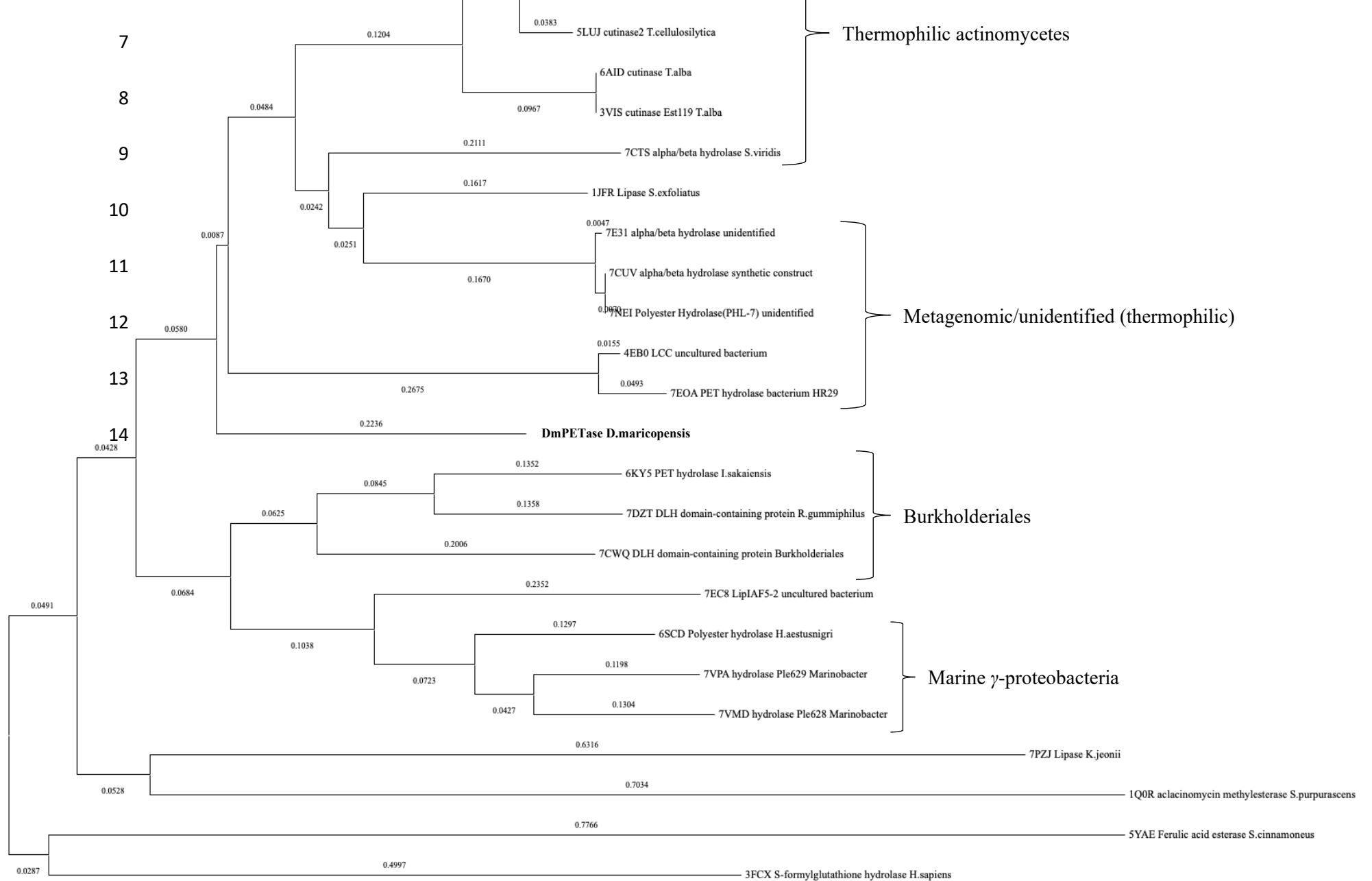
Figure S3 Evolutionary relationships of taxa: The evolutionary history was inferred using the Neighbor-Joining method [20]. The optimal tree is shown. The tree is drawn to scale, with branch lengths (next to the branches) in the same units as those of the evolutionary distances used to infer the phylogenetic tree. The evolutionary distances were computed using the Poisson correction method [21] and are in the units of the number of amino acid substitutions per site. This analysis involved 25 amino acid sequences. All ambiguous positions were removed for each sequence pair (pairwise deletion option). There was a total of 301

Supplementary Material
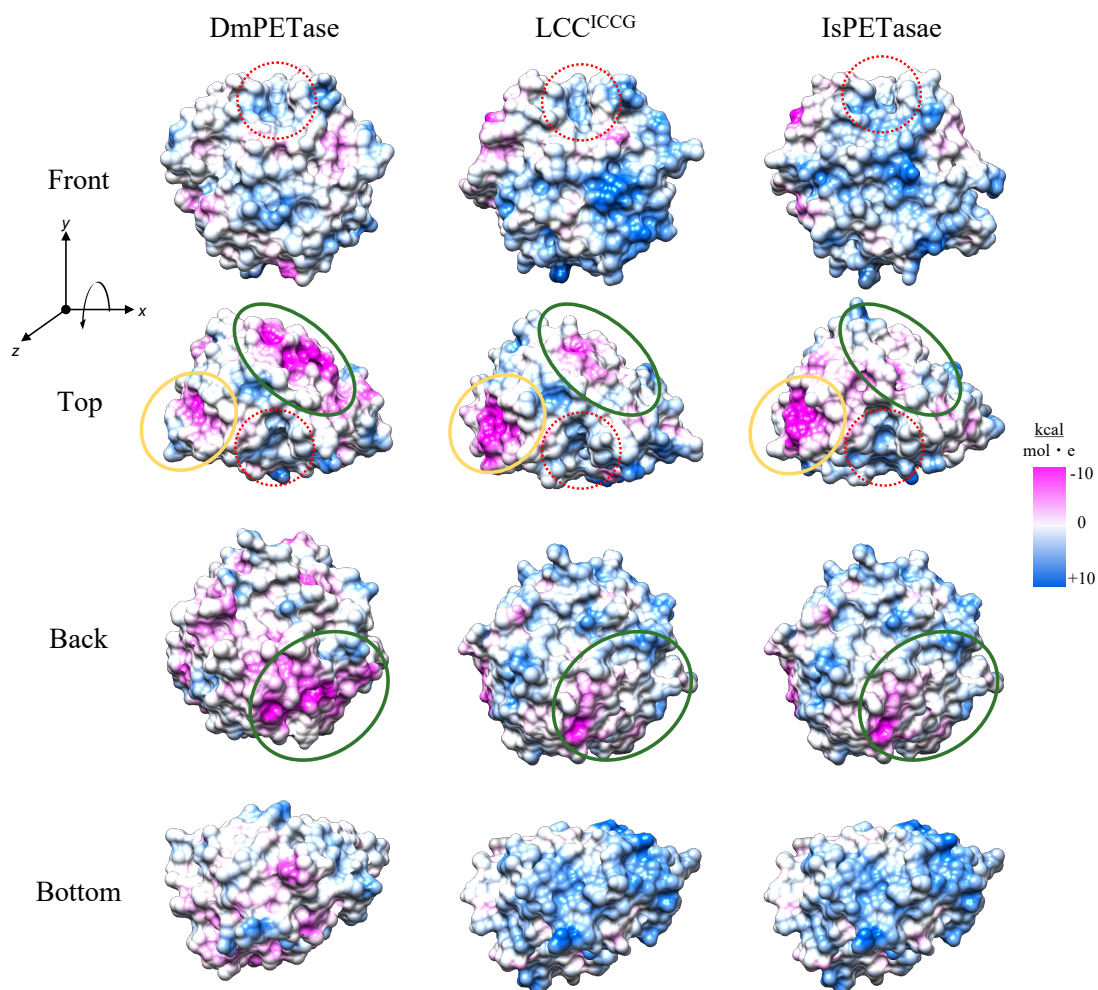
Figure S4 Electrostatic (Coulomb) potential distribution mapped to the solvent-accessible surface of *Dm*PETase, LCC[ICCG] and *Is*PETase structures. The colors represent negative charges in pink and positive charges in blue, with a scale in kcal·mol^{-1}·e^{-1}. The front side of the enzymes was determined the one, where the active-site cleft (in red dashed circles) is on the top. The models were then flipped 90° along the x-axis three times to display all sides of the enzymes.
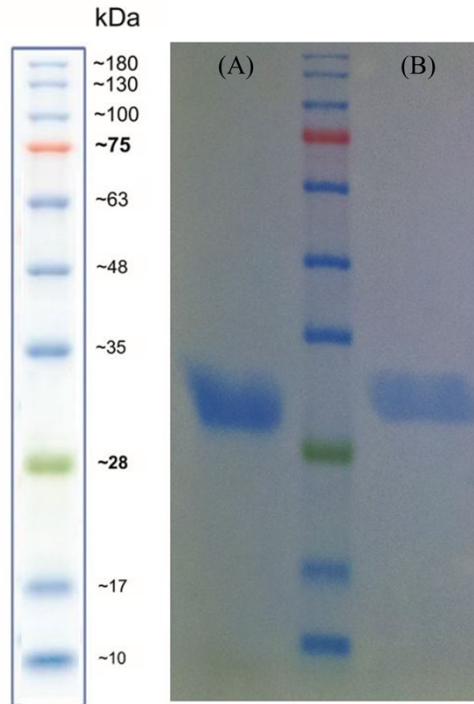
Figure S5 SDS-PAGE gel (12 % w/w) of LCC^{ICCG} (A) and *Dm*PETase (B).
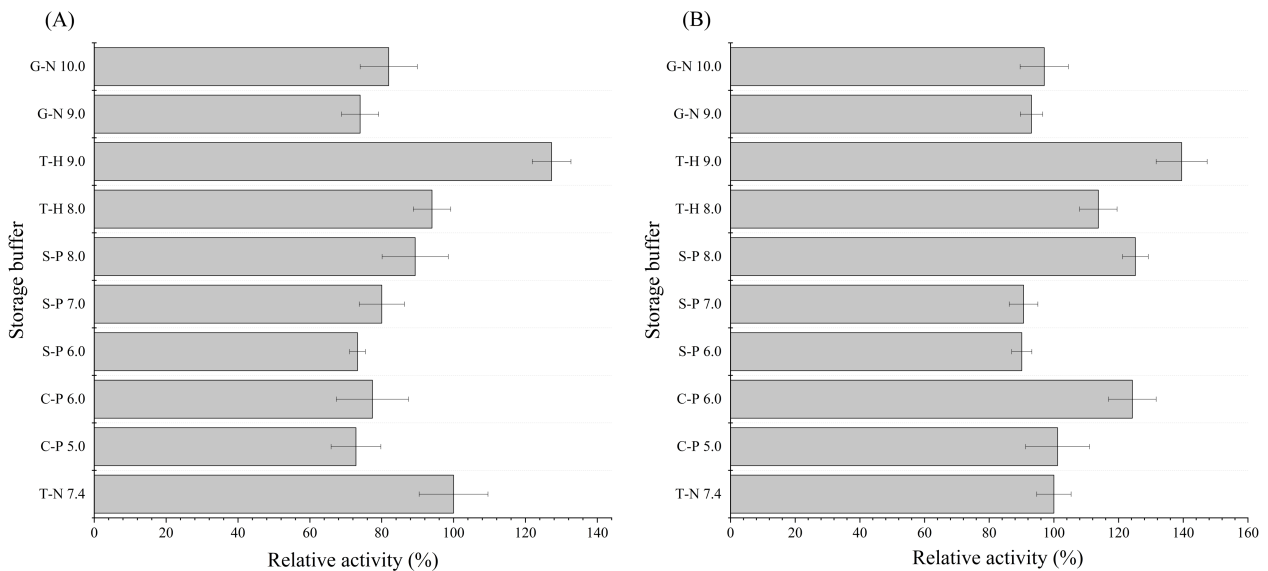
Figure S6 Effect of pH on the stability of *Dm*PETase (A) and LCC^{ICCG} (B). Relative activity

was defined after assaying *Dm*PETase and LCC^{ICCG}, which were incubated at 4 °C in a

variety of buffers for 3 days, with 1 mM *p*NPB in 0.1 M phosphate-citrate buffer (pH 6.0), at

35 °C. Different storage buffer systems used were standard storage buffer 0.025 M Tris-HCl,

0.15 M NaCl (T-H, pH 7.4), 0.2 M citrate-phosphate (C-P, pH 3.0-6.0), 0.2 M sodium-

30 phosphate (S-P, pH 6.0-8.0), 0.2 M Tris-HCl (T-H, pH 8.0-9.0) and 0.2 M glycine-NaOH (G-

31 N, pH 9.0-10.0).

32
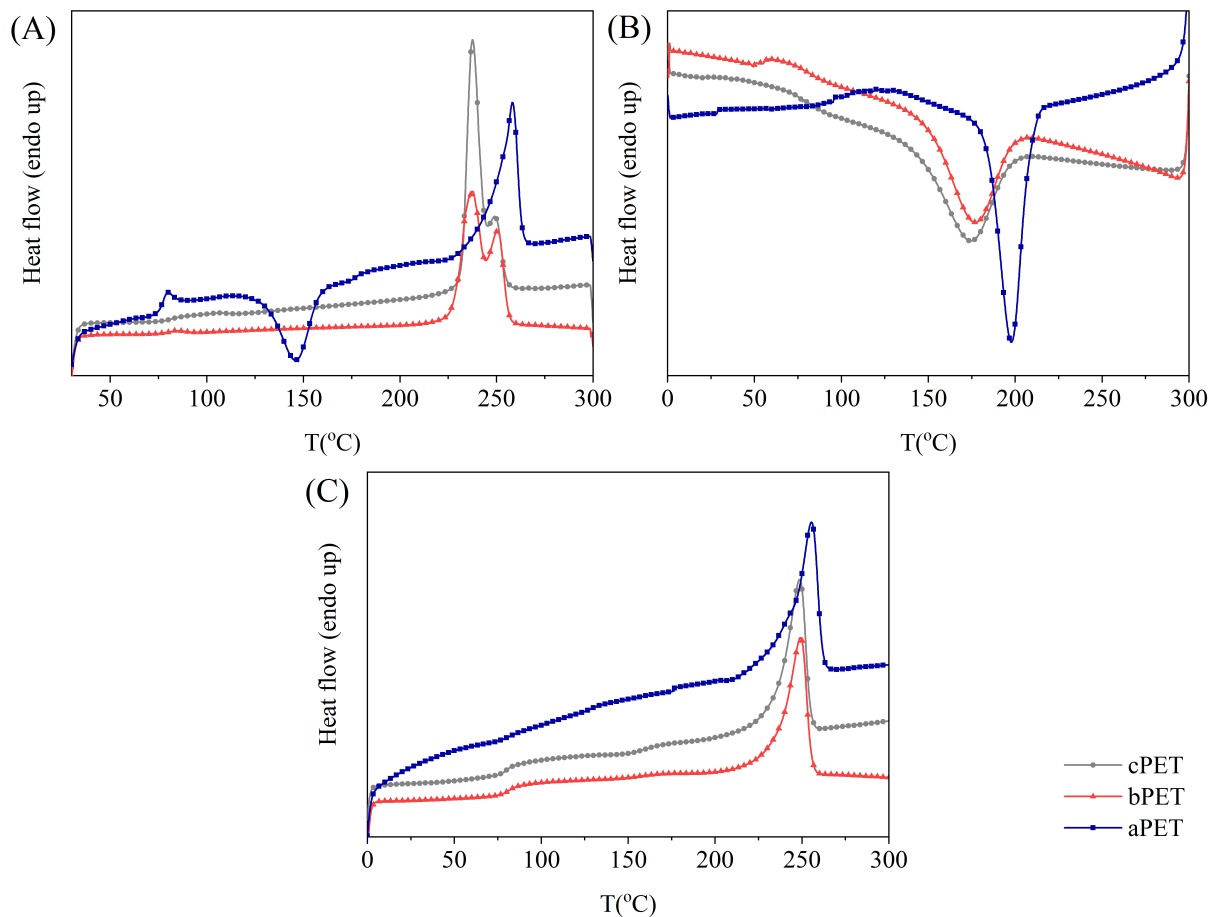
33

34 **Figure S7** First heating (A), cooling (B) and second heating (C) of the virgin powders cPET,

35 bPET and aPET.

Supplementary Material
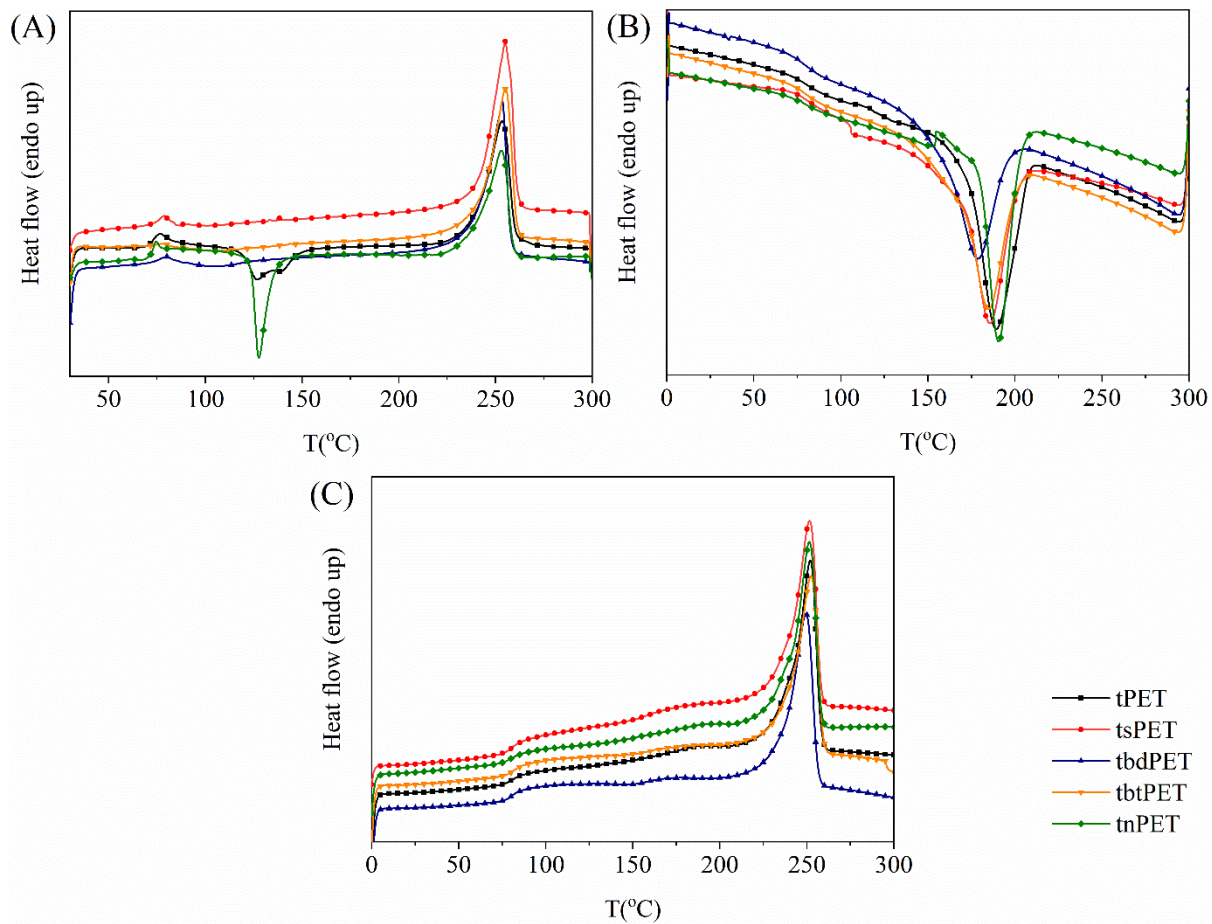
Figure S8 First heating (A), cooling (B) and second heating (C) of the post-consumer transparent bottle compartments (tnPET, tsPET, tbdPET, tbtPET) and powder (tPET).

Supplementary Material
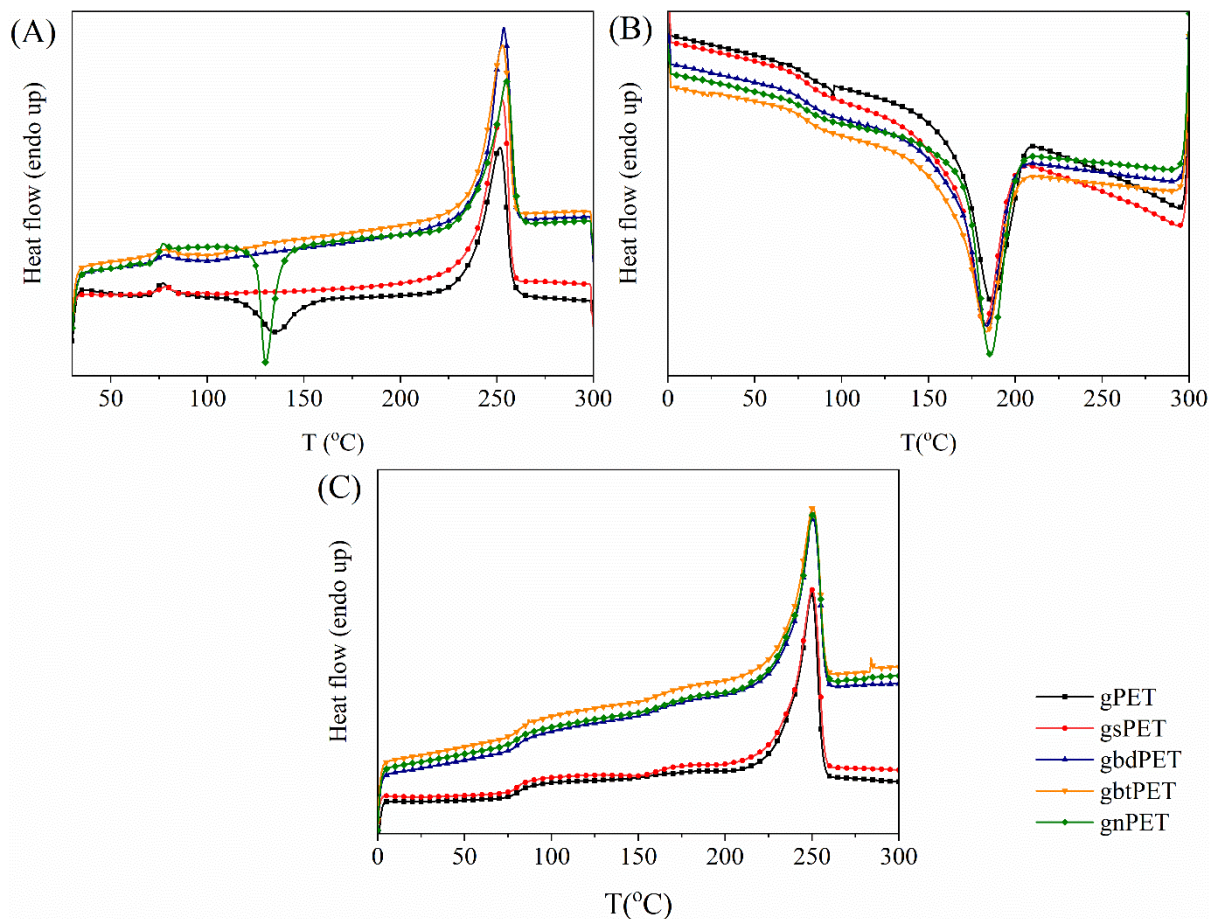
Figure S9 First heating (A), cooling (B) and second heating (C) of the post-consumer green bottle compartments (gnPET, tsPET, tbdPET, tbtPET) and powder (gPET).
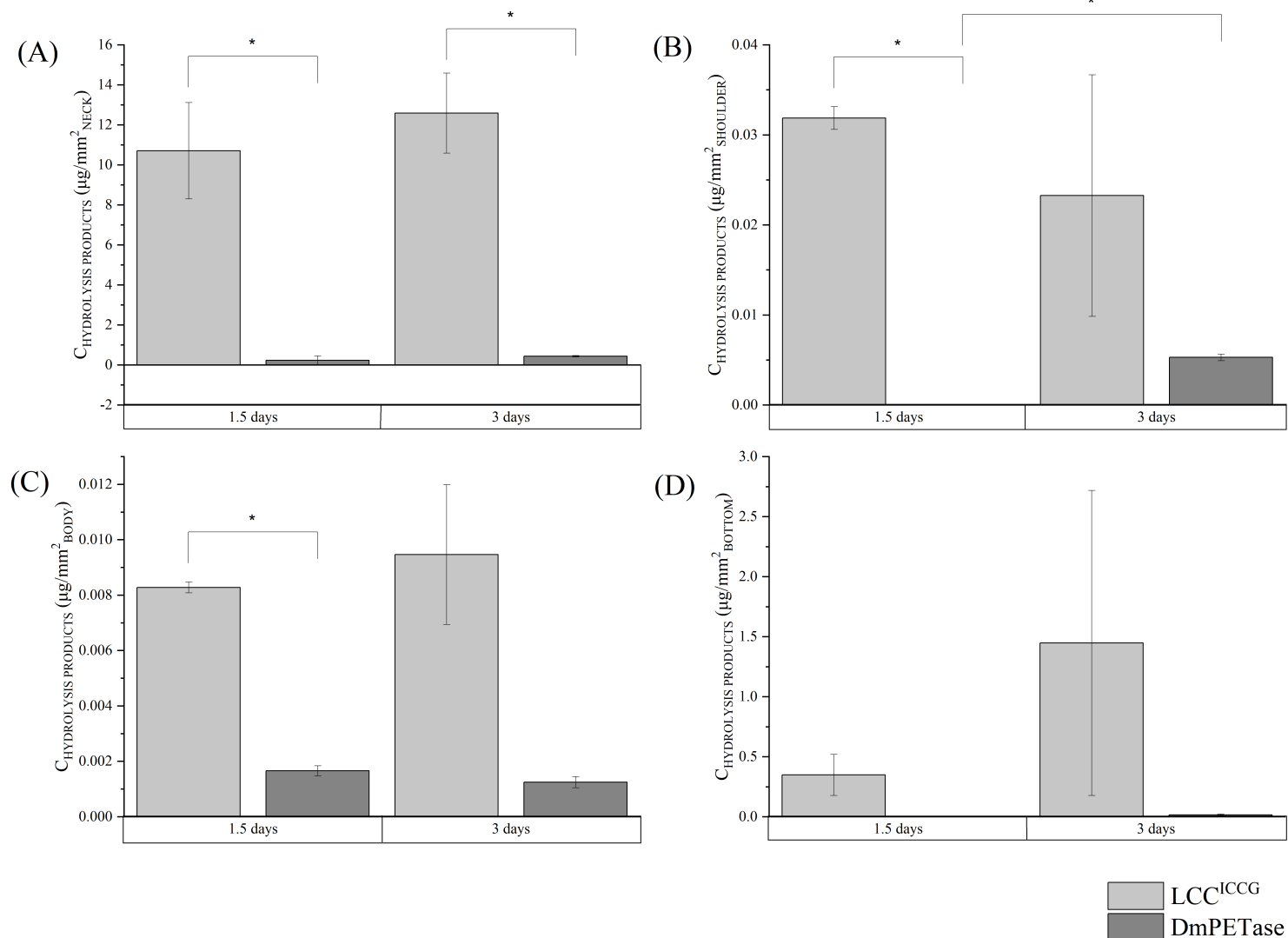
Figure S10 Water-soluble products released after treating different compartments of a transparent post-consumer PET bottle with *Dm*PETase (dark grey) and LCC^{ICCG} (light grey). Transparent PET bottle samples: Neck of x_c 13% (A), shoulder of x_c 31% (B), body of x_c 30% (C) and bottom of x_c 29% (D). Reactions took place at 50 °C for 72 h. Asterisk brackets represent statistically significant differences between corresponding values, according to Independent-Samples t-Test with a significance level of p-value < 0.05.
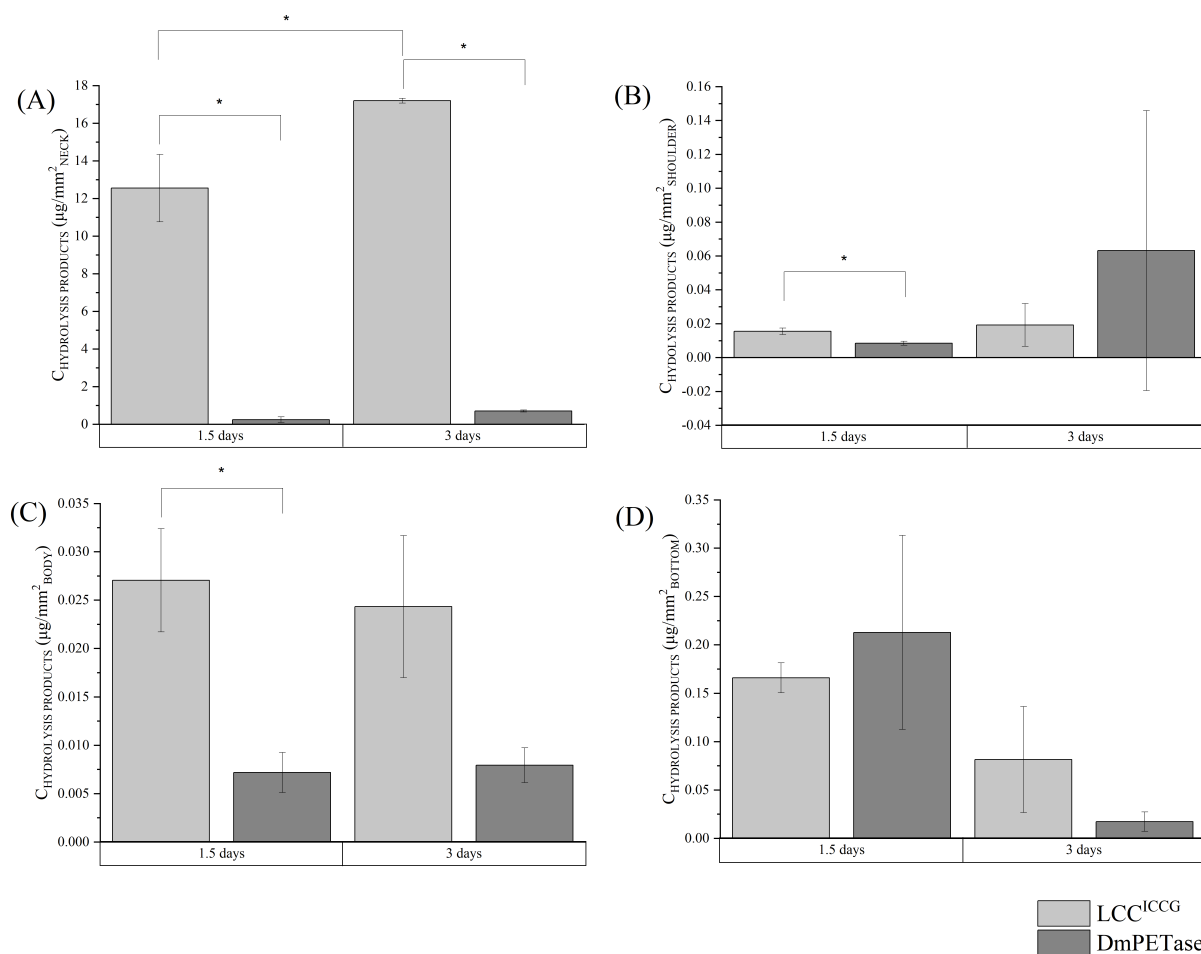
Figure S11 Water-soluble products released after treating different compartments of a green post-consumer PET bottle with DmPETase (dark grey) and LCC^{ICCG} (light grey). Green PET bottle samples: Neck of x_c 13% (A), shoulder of x_c 31% (B), body of x_c 30% (C) and bottom of x_c 29% (D). Reactions took place at 50 °C for 72 h. Asterisk brackets represent statistically significant differences between corresponding values, according to Independent-Samples t-Test with a significance level of p-value < 0.05.
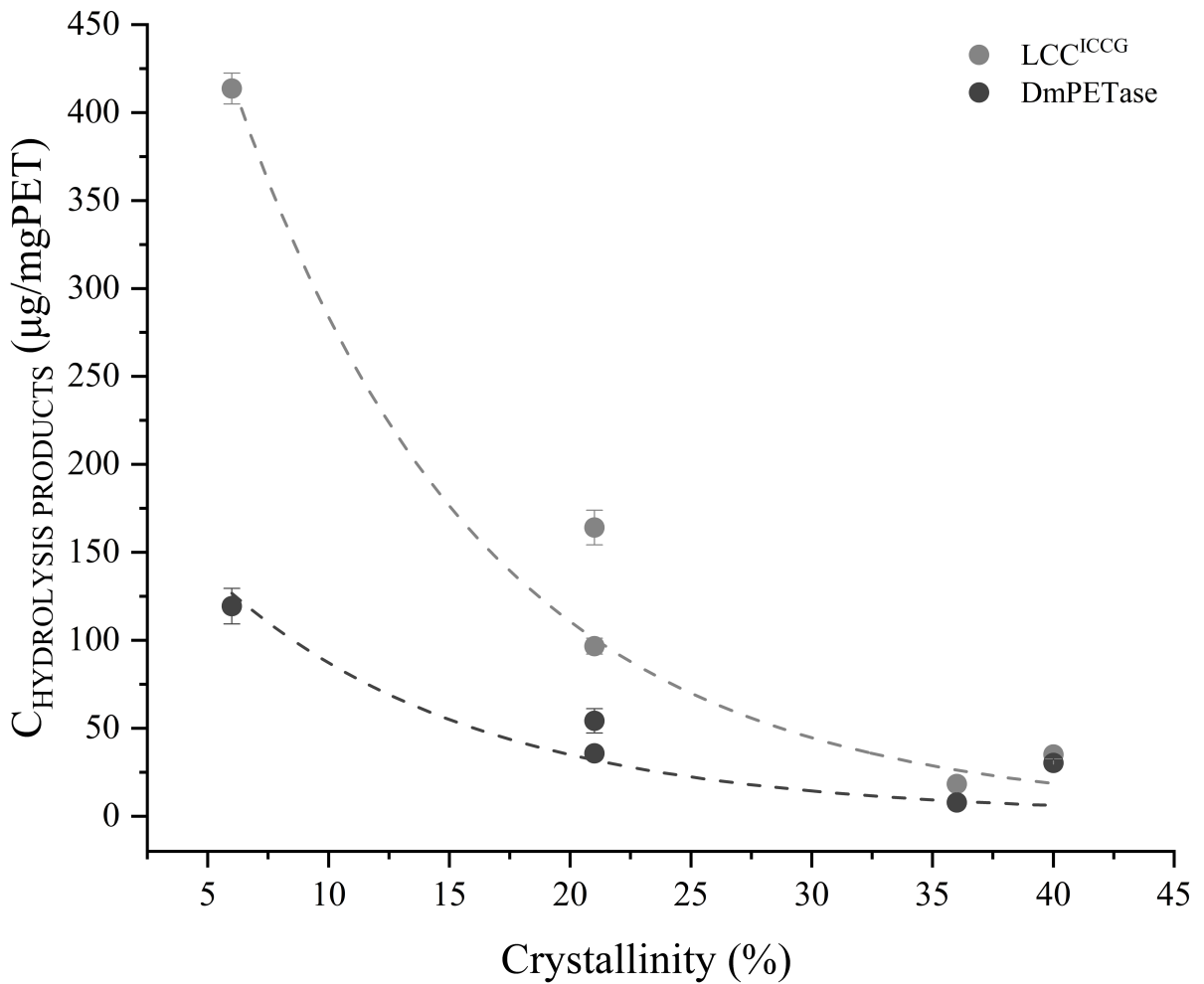
Figure S12 Concentration of released hydrolysis products by enzymatic treatment of PET samples of variable crystallinity degrees (6-40 %) with *Dm*PETase and LCC[ICCG].

Supplementary Material

58   **Table S1** Thermal properties of the various tested PET materials.

Sample	1st heating						Cooling			2nd heating			
	T_{g1} (°C)	T_{cc} (°C)	ΔH_{cc1} (J/g)	T_{m1} (°C)	ΔH_{m1} (J/g)	x_{c1} (%)	T_c (°C)	ΔH_c (J/g)	x_c (J/g)	T_{g2} (°C)	T_{m2} (°C)	ΔH_m (J/g)	x_{c2} (%)
cPET	81±2			237±1 249±0	55±5	40±3	174±0	37±4	26±3	79±1	248±1	35±3	25±2
bPET	82±0			237±1 250±0	51±3	36±2	177±1	32±2	23±1	81±0	249±0	33±1	24±1
aPET	77±2	145±2	30±4	256±3	39±2	6±2	197±1	51±9	37±7	nd*	253±3	39±4	28±3
tnPET	73±0	128±0	19±2	255±2	33±2	10±0	189±2	33±2	23±2	81±1	252±1	34±1	24±1
tsPET	75±2			254±2	43±4	31±3	184±2	33±3	23±2	80±1	250±2	33±3	24±2
tbdPET	76±1			253±1	43±5	31±3	179±1	31±0	22±0	81±1	250±0	33±2	24±1
tbtPET	75±1			255±0	43±4	31±3	185±0	35±0	25±0	81±1	252±0	34±3	24±2
tPET	74±1	127±0	12±3	253±0	42±4	21±5	188±2	34±0	25±0	81±1	251±1	35±0	25±0
gnPET	73±1	129±2	19±0	254±1	34±3	11±2	188±4	33±2	23±1	80±0	251±0	34±1	25±0
gsPET	75±0			253±0	44±1	31±1	184±2	32±1	23±1	80±1	250±0	40±7	29±5
gbdPET	74±2			253±0	44±2	31±2	184±1	37±2	27±2	80±0	251±0	34±1	24±1
gbtPET	73±1			253±0	38±4	27±3	185±2	31±5	22±4	80±0	250±0	32±3	23±2
gPET	74±0	135±1	11±2	251±0	40±0	21±1	186±0	34±2	24±1	80±0	250±0	36±1	26±1

59   * Not determined.

Supplementary Material

60   **Table S2** Thermal properties and average molecular weights of target PBS, PCL, PHB, PLA and PU powders.

| Polymer powder | DSC properties[1] | | | | | | | | | | | TGA properties[1] | | | Average molecular weights[2] | | |
| | 1st heating | | | Cooling | | | | 2nd heating | | | | | | | | | |
	T_{m1} (°C)	ΔH_{f1} (J/g)	x_C (%)	T_c (°C)	ΔH_c (J/g)	T_g (°C)	T_{cc} (°C)	ΔH_{cc} (J/g)	T_{m2} (°C)	ΔH_{f2} (J/g)	x_C (%)	$T_{d,5\%}$ (°C)	T_d (°C)	Char (%)	$\overline{M_n}$ (kg/mol)	$\overline{M_w}$ (kg/mol)	PDI
PCL	63	80	58	30	62	-64	–	–	56	63	45	365	397	3	80.7 ± 9.0	118.2 ± 2.7	1.5 ± 0.1
PLA	156	29	31	–	–	59	114	1	152	12	11	320	356	2	49.2 ± 3.3	100.7 ± 15.2	2.0 ± 0.2
PBS	115	81	66	83	78	-32	101	7	109, 115	78	64	333	387	2	12.8 ± 0.1	27.4 ± 0.1	2.2 ± 0.0
PHB	170	74	51	113	64	-4	–	–	160, 168	72	49	254	277, 370	4	32.4 ± 1.5	135.0 ± 3.5	4.2 ± 0.1
PU	–	–	–	53	3	150	–	–	–	–	–	303	343, 397	14	66.3 ± 0.3	128.5 ± 2.2	2.0 ± 0.0

61   [1]: [19] [2]: Defined by GPC analysis.

Supplementary Material

62 **Table S3** Average molecular weights of different synthetic polymers before and after
63 enzymatic treatment with *Dm*PETase and LCC[ICCG].

| Polymer powder | Average molecular weights before enzymatic treatment | | Average molecular weights after enzymatic treatment | | | |
| | | | *Dm*PETase | | LCC[ICCG] | |
	$\overline{M_n}$ (kg/mol)	$\overline{M_w}$ (kg/mol)	$\overline{M_n}$ (kg/mol)	$\overline{M_w}$ (kg/mol)	$\overline{M_n}$ (kg/mol)	$\overline{M_w}$ (kg/mol)
PCL	80.7 ± 9.0	118.2 ± 2.7	73.2 ± 1.9	115.0 ± 1.9	ND*	ND*
PBS	12.8 ± 0.1	27.4 ± 0.1	12.8 ± 0.1	27.4 ± 0.1	12.8 ± 0.1	27.4 ± 0.1
PHB	32.4 ± 1.5	135.0 ± 3.5	32.4 ± 1.5	135.0 ± 3.5	3.2 ± 1.5	135.0 ± 3.5
PLA	49.3 ± 3.3	100.7 ± 15.2	49.3 ± 3.3	100.7 ± 15.2	49.3 ± 3.3	100.7 ± 15.2
PU	66.3 ± 0.3	120.8 ± 2.2	60.9 ± 3.2	121.2 ± 7.9	63.4 ± 1.7	127.2 ± 1.1

64 *Not determined (not enough residual polymer sample).

Supplementary Material

References

[1]   E. Gasteiger, C. Hoogland, A. Gattiker, S. Duvaud, M.R. Wilkins, R.D. Appel, A. Bairoch, Protein Identification and Analysis Tools on ExPASy Server, in: J.M. Walker (Ed.), Proteomics Protoc. Handb., 1st ed., Humana Totowa, NJ, 2005: pp. 571–607. https://doi.org/10.1385/1592598900.

[2]   F.A. Rainey, K. Ray, M. Ferreira, B.Z. Gatz, F. Nobre, D. Bagaley, B.A. Rash, M.J. Park, A.M. Earl, N.C. Shank, A.M. Small, M.C. Henk, J.R. Battista, P. Kämpfer, M.S. Da Costa, Erratum: Extensive diversity of ionizing-radiation-resistant bacteria recovered from Sonoran desert soil and description of nine new species of the genus Deinococcus obtained from a single soil sample (Applied Environmental Microbiology (2005) 71, 9 (5225, Appl. Environ. Microbiol. 71 (2005) 7630. https://doi.org/10.1128/AEM.71.11.7630.2005.

[3]   F. V Ranzoni, Fungi Isolated in Culture from Soils of the Sonoran Desert, Mycologia. 60 (1968) 356–371.

[4]   L. Su, K. Chen, S. Bai, L. Yu, Y. Sun, Cutinase fused with C-terminal residues of α-synuclein improves polyethylene terephthalate degradation by enhancing the substrate binding, Biochem. Eng. J. 188 (2022) 108709. https://doi.org/10.1016/j.bej.2022.108709.

[5]   T.B. Thomsen, C.J. Hunt, A.S. Meyer, Influence of substrate crystallinity and glass transition temperature on enzymatic degradation of polyethylene terephthalate (PET), N. Biotechnol. 69 (2022) 28–35. https://doi.org/10.1016/j.nbt.2022.02.006.

[6]   E. Nikolaivits, M. Kanelli, M. Dimarogona, E. Topakas, A middle-aged enzyme still in its prime: Recent advances in the field of cutinases, Catalysts. 8 (2018). https://doi.org/10.3390/catal8120612.

[7]   N. Mohanan, Z. Montazer, P.K. Sharma, D.B. Levin, Microbial and Enzymatic Degradation of Synthetic Plastics, Front. Microbiol. 11 (2020). https://doi.org/10.3389/fmicb.2020.580709.

[8]   S. Giraldo-Narcizo, N. Guenani, A.M. Sánchez-Pérez, A. Guerrero, Accelerated Polyethylene Terephthalate (PET) Enzymatic Degradation by Room Temperature

Supplementary Material

Alkali Pre-treatment for Reduced Polymer Crystallinity, ChemBioChem. 24 (2023) 1–6. https://doi.org/10.1002/cbic.202200503.

[9]   S. Kaabel, J.P. Daniel Therien, C.E. Deschênes, D. Duncan, T. Friščic, K. Auclair, Enzymatic depolymerization of highly crystalline polyethylene terephthalate enabled in moist-solid reaction mixtures, Proc. Natl. Acad. Sci. U. S. A. 118 (2021) 1–6. https://doi.org/10.1073/pnas.2026452118.

[10] R. Wei, D. Breite, C. Song, D. Gräsing, T. Ploss, P. Hille, R. Schwerdtfeger, J. Matysik, A. Schulze, W. Zimmermann, Biocatalytic Degradation Efficiency of Postconsumer Polyethylene Terephthalate Packaging Determined by Their Polymer Microstructures, Adv. Sci. 6 (2019). https://doi.org/10.1002/advs.201900491.

[11] D. Gercke, C. Furtmann, I.E.P. Tozakidis, J. Jose, Highly Crystalline Post-Consumer PET Waste Hydrolysis by Surface Displayed PETase Using a Bacterial Whole-Cell Biocatalyst, ChemCatChem. 13 (2021) 3479–3489. https://doi.org/10.1002/cctc.202100443.

[12] R. Panowicz, M. Konarzewski, T. Durejko, M. Szala, M. Łazi, Properties of Polyethylene Terephthalate (PET) after, (2021).

[13] Y. Kong, J.N. Hay, Multiple melting behaviour of poly(ethylene terephthalate), Polymer (Guildf). 44 (2002) 623–633. https://doi.org/10.1016/S0032-3861(02)00814-5.

[14] P.J. Holdsworth, A. Turner-Jones, The melting behaviour of heat crystallized poly(ethylene terephthalate), Polymer (Guildf). 12 (1971) 195–208. https://doi.org/10.1016/0032-3861(71)90045-0.

[15] H. Gu, F. Alfayez, T. Ahmed, Z. Bashir, Poly (ethylene terephthalate) Powder — A Versatile, Polymers (Basel). (2019).

[16] C. Bach, X. Dauchy, S. Etienne, Characterization of poly(ethylene terephthalate) used in commercial bottled water, IOP Conf. Ser. Mater. Sci. Eng. 5 (2009). https://doi.org/10.1088/1757-899X/5/1/012005.

[17] M. Fereydoon, S.H. Tabatabaei, A. Ajji, Effect of uniaxial stretching on thermal, oxygen barrier, and mechanical properties of polyamide 6 and poly(m-xylene adipamide) nanocomposite films, Polym. Eng. Sci. 55 (2015) 1113–1127.

Supplementary Material

123   https://doi.org/10.1002/pen.23982.

124 [18] B.L. Wadey, Plasticizers US5281647 Polymeric plasticizers, Addit. Polym. 1994 (1994)
125   4. https://doi.org/10.1016/0306-3747(94)90539-8.

126 [19] E. Nikolaivits, G. Taxeidis, C. Gkountela, S. Vouyiouka, V. Maslak, J. Nikodinovic-
127   Runic, E. Topakas, A polyesterase from the Antarctic bacterium Moraxella sp. degrades
128   highly crystalline synthetic polymers, J. Hazard. Mater. 434 (2022) 128900.
129   https://doi.org/10.1016/j.jhazmat.2022.128900.

130 [20] N. Saitou, M. Nei, The neighbor-joining method: a new method for reconstructing
131   phylogenetic   trees.,   Mol.   Biol.   Evol.   4   (1987)   406–425.
132   https://doi.org/10.1093/oxfordjournals.molbev.a040454.

133 [21] Z. Emile, P. Linus, Evolutionary Divergence and Convergence in Proteins, Europhys.
134   Lett. 42 (1998) 167–172. https://doi.org/10.1209/epl/i1998-00224-x.

135 [22] K. Tamura, G. Stecher, S. Kumar, MEGA11: Molecular Evolutionary Genetics Analysis
136   Version   11,   Mol.   Biol.   Evol.   38   (2021)   3022–3027.
137   https://doi.org/10.1093/molbev/msab120.

138 [23] G. Stecher, K. Tamura, S. Kumar, Molecular evolutionary genetics analysis (MEGA)
139   for   macOS,   Mol.   Biol.   Evol.   37   (2020)   1237–1239.
140   https://doi.org/10.1093/molbev/msz312.

141